

PAPER

[View Article Online](#)
[View Journal](#) | [View Issue](#)Cite this: *Polym. Chem.*, 2022, **13**, 3768Antimicrobial 'inks' for 3D printing: block copolymer-silver nanoparticle composites synthesised using supercritical CO₂†Ryan R. Larder,^a Eduards Krumins,^{a,b} Philippa L. Jacob,^a Kristoffer Kortsen,^a Robert Cavanagh,^c Long Jiang,^c Claudia Vuotto,^d Iolanda Francolini,^e Christopher Tuck,^b Vincenzo Taresco^{b,*a} and Steven M. Howdle^{b,*a}

Silver nanoparticles (AgNP) are widely exploited for their effective antimicrobial activity against a range of pathogens. Their high efficacy in this regard has seen the global demand for AgNP in consumer products steadily increase in recent years, necessitating research into novel low environmental impact synthesis approaches. Here we present a new synthetic methodology to produce polymer-AgNP composite microparticles using supercritical carbon dioxide (scCO₂) and avoiding use of any petrochemically derived solvents. Poly(methyl methacrylate)-poly(4-vinylpyridine) (PMMA-*b*-P4VP) block copolymers were synthesised via RAFT-mediated dispersion polymerisation in scCO₂, with *in situ* thermal degradation of various amounts of a CO₂-soluble silver complex. Selective interaction of the silver with the pyridinyl moieties of the block copolymer allowed the formation of AgNP, dispersed within the block copolymer microparticles, leading to homogeneous composites. The by-products of the reaction were also removed by extracting with a flow of CO₂ to yield a clean dry product in a single process. The composites were found to be non-cytotoxic and proved to have good antimicrobial activity against two bacterial strains. Though no significant activity was seen for at least the first 24 hours, inhibition of bacterial growth afterwards proved to be extremely persistent, with inhibition observed even after 15 days. Finally, the microparticulate nature of the synthesised composites was exploited and tested for compatibility in the Laser Sintering (LS) 3D printing process. Composite microparticles were fused to produce solid objects, without aggregation of the AgNP. With further optimisation, these composites could prove to be an incredibly versatile 'ink' that may be used within additive manufacturing and 3D printing to rapidly produce bespoke medical devices with inherent antimicrobial activity.

Received 30th March 2022,
Accepted 6th June 2022

DOI: 10.1039/d2py00398h

rsc.li/polymers

Introduction

Silver nanoparticles (AgNP) have been the focus of much research over the past few decades, owing to their unique optical, electrical and biological properties.^{1,2} This has allowed their application in sensing,³ catalysis,⁴ electronics⁵ and, probably most notably, in antimicrobial materials.⁶ Due to the high

surface area to volume ratio and unique mechanisms of action, AgNP have proven to have remarkable antimicrobial activity against a range of pathogens, including SARS-CoV-2.^{7,8} It is this particular property that has led to AgNP now being found in a growing range of consumer goods such as cosmetics, cleaning sprays, textiles and dentistry products.⁹ Consequently, production of AgNP is projected to grow significantly in the coming years and new green synthetic methodologies will be required to limit the environmental impact of their increased manufacture.¹⁰

Some of the more common methods to fabricate AgNP include chemical synthesis by reduction of dissolved silver ions to elemental nanoparticles, or physical methods such as laser ablation of bulk silver.¹¹ However, these methods generally require the use of non-renewable and toxic chemicals or excessive amounts of energy, carrying with them high environmental costs. Many recent publications outline more sustainable methods to synthesise AgNP such as using bio-sourced

^aSchool of Chemistry, The University of Nottingham, University Park, Nottingham, NG7 2RD, UK. E-mail: vincenzo.taresco@nottingham.ac.uk, steve.howdle@nottingham.ac.uk

^bCentre for Additive Manufacturing, Faculty of Engineering, University of Nottingham, Nottingham, NG7 2RD, UK

^cSchool of Pharmacy, The University of Nottingham, University Park, Nottingham, NG7 2RD, UK

^dMicrobial Biofilm Laboratory, IRCCS Fondazione Santa Lucia, 00143 Rome, Italy

^eDepartment of Chemistry, Sapienza University of Rome, 00185 Rome, Italy

† Electronic supplementary information (ESI) available. See DOI: <https://doi.org/10.1039/d2py00398h>



molecules to reduce silver or the use of supercritical fluid solvents. These methods have been reviewed extensively and can be found elsewhere.^{12–16}

Another important consideration for the manufacture of AgNP is their stability and storage. Aqueous dispersions of AgNP with polymeric stabilisers can be prone to aggregation or oxidation if handled incorrectly.^{17,18} For increased stability and to allow their functionality to be utilised for end applications, AgNP are often deposited onto the surface of substrates. Ideally, the synthesis of AgNP and deposition onto substrates should be combined into a single process to negate the complications in storing and transporting neat AgNP, as well as eliminating costly additional synthetic steps.

Previously, we have demonstrated that this can be achieved with low environmental impact using supercritical CO₂ (scCO₂).^{19,20} Certain silver complexes can be dissolved in scCO₂, deposited in the outer layers of polymeric substrates such as polyamide or polycarbonate and then reduced to yield AgNP decorating the surface of the substrate.^{21,22} A similar methodology has also been applied to decorate the surface of poly(methyl methacrylate) (PMMA) microparticles with AgNP.²³

Despite the advantages of this approach to manufacturing AgNP-based materials, there are still some limitations. Foremost being that the desired AgNP substrate must be synthesised first in a separate process and with small enough dimensions that it is able to fit into the high-pressure vessel for processing. Furthermore, this scCO₂ deposition approach, like many other methodologies, only serves to deposit AgNP on the outer layers of substrates. In applications where AgNP are released to combat the spread of microorganisms, these AgNP are often released in a short burst and the overall antimicrobial effect might only be short lived.

In this paper we propose a new and facile approach to produce polymeric-AgNP composite microparticles that tackle these shortcomings. We have recently shown that scCO₂ is an effective medium to produce nanostructured block copolymer microparticles, using reversible addition–fragmentation chain transfer (RAFT) mediated dispersion polymerisation, with minimal environmental impact.^{24–26} Here, we perform this controlled polymerisation concurrently with the thermal degradation of a scCO₂-soluble silver complex to produce AgNP, deposited homogeneously throughout the polymeric substrate. The synthesised block copolymer consists of a PMMA and poly(4-vinylpyridine) (P4VP) block. This particular block copolymer has already been successfully used as a structural template for the fabrication of polymer-inorganic composites, owing to the selective coordinative bonding ability of the pyridinyl nitrogen.^{27,28} In this approach, the 4VP monomer is combined in scCO₂ with the dissolved silver precursor to allow incorporation of AgNP throughout the formed block copolymer microparticles. The resulting polymer-AgNP composite powders were tested for their biocompatibility and antimicrobial activity over an extended time-period.

Moreover, as a microparticulate powder, the composites also lend themselves well for use in additive manufacturing

techniques such as Laser Sintering (LS), where polymeric materials can be fused to create arbitrary 3D objects.²⁹ Recently, LS has been used to produce antimicrobial polymeric objects through the mixing of commercially available polymers with bulk antimicrobial glasses.³⁰ Direct printing of a single composite ink that possesses the broad biocidal properties of AgNP would greatly broaden the scope of this manufacturing approach. As such, the PMMA-*b*-P4VP-AgNP composite was also trialled for use as a potential ‘ink’ in the LS process to produce solid objects. The morphology of the objects was analysed to determine the distribution of AgNP in the final construction.

Overall, the production of AgNP-based components can be realised in a simple process and with low environmental cost. The synthesis approach offers a facile way to produce stable AgNP-based materials from basic chemical feedstocks without the need for any toxic or non-renewable solvents. The antimicrobial materials can then be used in additive manufacturing to create custom designed objects on demand to suit the needs of the desired application.

Experimental

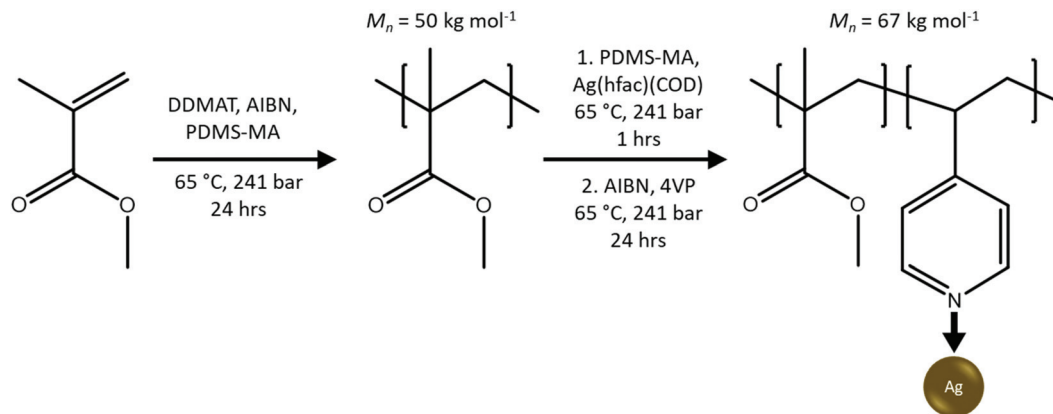
Materials

Methyl methacrylate (MMA, ProSciTech, 99%) and 4-vinylpyridine (4VP, Acros Organics, 95%) were purified by eluting through a basic alumina column to remove inhibitor. 2,2'-Azobis(2-methylpropionitrile) (AIBN, Sigma Aldrich, 98%) was purified by recrystallisation from methanol. (1,5-Cyclooctadiene)(hexafluoroacetylacetonato)silver(i) (Ag(hfac)(COD), Sigma Aldrich, 99%), dry CO₂ (BOC, SFC grade, 99.99%), 2-(Dodecylthiocarbonothioylthio)-2-methylpropionic acid (DDMAT, Sigma Aldrich, 98%) and poly(dimethylsiloxane) monomethyl methacrylate (PDMS-MA, Fluorochem, $M_n \sim 10$ kg mol⁻¹) were all used as received.

Synthesis of PMMA-*b*-P4VP-AgNP composite

Block Copolymer composites were synthesised using a two-pot seeded dispersion method in an in-house built scCO₂ autoclave (Scheme 1), similar to methods reported in previous publications.^{28,31} Firstly, a 50 kg mol⁻¹ PMMA macro-RAFT agent was synthesised. MMA (10 g, 99.9 mmol), AIBN (16.4 mg, 0.10 mmol), DDMAT (72.8 mg, 0.20 mmol) and PDMS-MA polymeric stabiliser (0.5 g, $M_n \sim 10$ kg mol⁻¹) were mixed in a sealed vial and degassed by purging with argon for 30 minutes. Meanwhile, a 60 mL autoclave was degassed by flushing with CO₂ at 1–2 bar for 30 minutes. The monomer solution was added to the autoclave *via* syringe against a positive pressure of CO₂ to prevent the ingress of air. The autoclave was then sealed, pressurised to 50 bar and heated to 65 °C before further addition of CO₂ to the reaction pressure of 241 bar. After stirring at 300 rpm for 24 hours, the reaction was cooled to room temperature, slowly vented and the PMMA product collected as a white, fine free-flowing powder.





Scheme 1 Reaction scheme for the synthesis of a PMMA-*b*-P4VP block copolymer composite with AgNP, via a two-pot dispersion reaction in scCO_2 .

In the second reaction stage, the PMMA macro-RAFT agent (7.5 g), additional PDMS-MA (0.125 g) and variable amounts of $\text{Ag}(\text{hfac})(\text{COD})$ were loaded into the 60 mL autoclave and degassed by flushing with CO_2 at 1–2 bar for 30 minutes. The autoclave was then sealed, heated to 65 °C and pressurised to 241 bar, following the standard operating procedure. After stirring at 300 rpm for ~1 hour, a degassed solution of 4VP (2.5 g, 23.8 mmol) with AIBN (6.25 mg, 0.04 mmol) was added to the autoclave *via* a HPLC pump at a rate of 0.5 mL min^{-1} . After 24 hours the autoclave was cooled to 50 °C and the CO_2 inlet and outlet taps were opened slowly and simultaneously. A moderate flow of CO_2 was allowed to pass through the autoclave for 30 minutes, keeping the vessel pressure between approximately 138–201 bar, to remove any scCO_2 soluble impurities. After the CO_2 extraction, both inlet and outlet taps were closed simultaneously, and the autoclave was cooled to room temperature before slowly venting to atmospheric pressure. The PMMA-*b*-P4VP-AgNP composite product was collected as a light brown, dry free-flowing powder.

Cell culture

Caco-2 human adenocarcinomic colon epithelial cells were obtained from the American Type Culture Collection (ATCC; Manassas, Virginia) and used at passages 35–40. Caco-2 cells were cultured in Dulbecco's modified Eagle's medium (DMEM; Sigma-Aldrich) supplemented with 10% (v/v) fetal bovine serum (FBS; Sigma-Aldrich) and 2 mM L-glutamine (Sigma-Aldrich), and at 37 °C with 5% CO_2 .

Cytotoxicity measurements

The biocompatibility of PMMA-*b*-P4VP-AgNP composites was assessed by cytotoxicity tests on Caco-2 human intestinal epithelial cells. The Caco-2 cell line is a well-established model of the small intestine and was used to predicted potential toxicity of the materials following oral exposure. *In vitro* cytotoxicity assays were performed according to the protocol described in the ISO 10993-5 guide.³² Cells were seeded in a 12-well plate (Corning) at a density of 1.2×10^5 cells per well in 1 mL DMEM

with 10 vol% FBS. Cells were cultured for 24 hours before exposure to 1 mg of the selected PMMA-*b*-P4VP-AgNP composite suspended directly in 1 mL culture media per well for 48 hours. Metabolic activity was determined by exposure to PrestoBlue (Thermo Fisher Scientific) and cell membrane damage was assessed by a lactate dehydrogenase (LDH) release assay (Sigma-Aldrich, TOX7 kit). Triton X-100 (Sigma-Aldrich) applied at a concentration of 1 vol% was used as a positive control for cell death. Cells were exposed to no additional reagents for the negative control.

After exposure to the composite samples, 50 μL of supernatant was collected per well for LDH content analysis. Cells were then washed twice with phosphate-buffered saline (PBS) before adding 100 μL PrestoBlue reagent solution (10 vol% in phenol red free DMEM) per well for 60 min. The resulting fluorescence was measured at 560/600 nm ($\lambda_{\text{ex}}/\lambda_{\text{em}}$) on a Tecan Spark M10 multimode plate reader. Relative metabolic activity was calculated by setting measurements from the negative control as 100% activity and measurements from the positive control as 0% activity. LDH detection was performed according to the manufacturer's instructions, with 100 μL LDH reagent added to the collected supernatants before incubating in absence of light at room temperature for 25 min. Absorbance at 492 nm was then recorded. Relative LDH release was calculated with the negative control's absorbance taken as 0% and the positive control's taken as 100%, as it was assumed this caused total cell lysis.

Antimicrobial tests

Antimicrobial activity of the composites was determined by exposing bacteria to the aqueous suspensions of the dispersed samples. Samples were prepared as suspensions in sterile water at a concentration of 10 mg mL^{-1} . Samples (10 μL) of the supernatants were withdrawn from the suspensions at various timepoints. The supernatants were placed on Muller Hinton agar plates previously seeded with either *Staphylococcus aureus* (10850) or *Staphylococcus epidermidis* (ATCC 35984). Bacteria were seeded at an optical density of 0.05. Plates were incubated



at 37 °C for 18 hours and the activity of the samples was determined by measuring the size of the bacterial inhibition halo of each sample drop.

AgNP release studies

The release of AgNP from the polymer composite was tested in aqueous solutions. Samples of the PMMA-*b*-P4VP-AgNP composite (25 mg) were dispersed in distilled water (5 mL) or 4.7 pH buffer (5 mL, 0.1 M, acetic acid/sodium acetate) solutions. Small amounts (100 µL) of the mixture were removed at the desired timepoints and passed through a membrane filter (Millex, 0.45 µm) to remove any large polymer microparticles.

Laser Sintering of PMMA-*b*-P4VP-AgNP

Composite powders were printed into solid objects using an EOS Formiga P100 system equipped with a CO₂ laser (λ = 10.6 µm, spot size 200 µm). Thin square sections (20 × 20 × 0.5 mm) designed in Materialise Magics were printed. The PMMA-*b*-P4VP-AgNP powder was prepared by sieving through a 200 µm mesh filter and dried at 100 °C for one hour. The composite powder was then loaded onto the build platform and processed into thin sections using a bed temperature of 90 °C, hatching speed of 2500 mm s⁻¹, hatching distance of 0.25 mm, hatching laser power of 19 W and contour laser power of 19 W.

Characterisation

Nuclear magnetic resonance (¹H NMR) spectra were obtained using a Bruker AV-III 400 MHz spectrometer with samples dissolved in CDCl₃. Data was analysed using MestReNova software.

Gel permeation chromatography (GPC) was used to measure the molecular weight and dispersity of the PMMA macro-RAFT agents. An Agilent 1260 infinity SEC system was used with a Wyatt Optilab dRI detector. The mobile phase was a solvent mixture of chloroform and ethanol (9 : 1) with triethyl amine stabiliser (1% v/v). Samples were injected at a flow rate of 0.5 mL min⁻¹ and passed through a guard column followed by two separation columns (2 × Agilent PLgel 5 µm mixed C). The system was calibrated using PMMA narrow standards (M_n range: 0.5–2000 kg mol⁻¹).

Differential scanning calorimetry (DSC) was performed using a TA Instruments Q2000 DSC. 10 mg samples were heated to 200 °C (10 °C min⁻¹ ramp), cooled to -100 °C then reheated to 200 °C. Data was collected during the second heating run. T_g values were determined using TA universal analysis software.

Thermal gravimetric analysis (TGA) was performed using a TA Instruments Q500 TGA with platinum crucibles over a temperature range of 30 to 700 °C (10 °C min⁻¹ ramp) in air.

Scanning electron microscopy (SEM) was used to characterise the microstructure of composites as well as map their elemental composition. Samples were imaged using a JEOL 6490LV SEM equipped with an Oxford Instruments XMax 100TLE detector to simultaneously capture energy dispersive X-ray spectroscopy (EDXS) data. The average particle diameters

reported from SEM are a mean average of 100 measured particles (ImageJ processing software). Elemental maps were produced using an Aztec software package.

Transmission electron microscopy (TEM) images were captured using a JEOL 2100 + TEM at an accelerating voltage of 80 kV. Samples were prepared by embedding in an epoxy resin (Agar 100) at 50 °C for 48 hours before being cut into 100 nm thick sections using an RMC Powertome microtome equipped with a Diatome diamond knife.

UV/vis spectra for the PMMA-*b*-P4VP-AgNP composites were obtained by dissolving the composites in dichloromethane at a concentration of 3 mg mL⁻¹. Solutions were then analysed using a PerkinElmer Lambda 25 UV/vis spectrometer, scanning in the range of 250–600 nm.

Dynamic light scattering (DLS) was used to determine the size of the formed AgNP. A Zetasizer nano spectrometer (Malvern Instruments Ltd) equipped with a 633 nm laser at a fixed angle of 173° was used. Samples were equilibrated at 25 °C for 20 seconds prior to measuring. All measurements were an average of a total of 15 scans. The polydispersity index (PDI) was calculated as the square of the standard deviation divided by mean particle diameter for the relevant peaks.

Time-of-flight secondary ion mass spectrometry (ToF-SIMS) depth profile data were obtained using a ToF-SIMS IV instrument (ION-TOF GmbH, Münster, Germany). The measurements were performed in non-interlaced mode with 1 frame of analysis followed by 1 frame of sputter. The primary ion beam used for analysis was a bismuth liquid metal ion gun (Bi₃⁺) operated at 25 keV (pulsed target current of around 1 pA) and an argon gas cluster (Ar₁₇₀₀⁺, 10 keV) was used as the sputter source for depth profiling. Sputtering was performed over an area of 500 µm × 500 µm, with the central 200 µm × 200 µm area analysed at a 256 × 256 pixel resolution. Positive ion data were collected and the profiling data were analysed using SurfaceLab 7 software (IONTOF GmbH).

Results and discussion

Synthesis of PMMA-*b*-P4VP-AgNP composites

PMMA-*b*-P4VP block copolymers were synthesised in scCO₂ using a two-pot redispersion method (Scheme 1), that has been utilised in previous studies.³¹ The method uses a CO₂-soluble PDMS-MA polymeric stabiliser. This is well-known to facilitate the formation of block copolymer particles in scCO₂, yielding particle sizes around 1–3 µm when applied at a concentration of 5 wt% with respect to monomer mass.²⁴ The second stage of the polymerisation, whereby P4VP was polymerised using a PMMA microparticulate macro-RAFT agent, was performed while simultaneously forming AgNP in scCO₂ by thermal degradation of an inorganic precursor. Ag(hfac)(COD) was selected as the AgNP precursor material because of its solubility in scCO₂ and thermal degradation at the temperature used to perform the concurrent polymerisation.^{23,33} A two-pot approach to the formation of the composites was chosen purely due to practical limitation



in the high-pressure reaction system. In order to perform this reaction in a single pot, the Ag(hfac)(COD) would need to be added by a high-pressure solid addition device after polymerisation of the PMMA is complete. Such reactors have already been designed, and hence our synthesis may easily be further modified into a one-pot process if desired.³⁴

All PMMA-*b*-P4VP copolymers were synthesised with a target molecular weight of 67 kg mol⁻¹ and a target weight fraction of 25% P4VP. The quantity of AgNP precursor was varied between 62.5 to 250 mg per 10 g of total polymeric material to yield three composites. When concluding the reactions, the high-pressure mixtures were washed under a flow of CO₂ for 30 minutes prior to cooling and venting the autoclave. This additional extraction process was performed to remove any scCO₂-soluble components, such as unreacted monomer or displaced ligands. These materials could in principle be collected and recycled. The final cleaned composites were obtained as brown coloured fine powders. The colour is typical for the formation of AgNP, owing to surface plasmon resonances.³⁵ The composition and purity of the materials was assessed by ¹H NMR (Fig. S1†), with relevant data summarised in Table 1.

The ¹H NMR spectra indicated the successful formation of a PMMA-*b*-P4VP copolymer in all the reactions. Moreover, the successful extraction of the reaction impurities and by-products was confirmed by an absence of any peaks in the region of 4.0–6.0 ppm. This relates to protons in any unreacted 4VP or MMA monomers, as well as the displaced cyclooctadiene and hexafluoroacetylacetone ligands. The spectra suggested these compounds were not present in the resulting composites at any significant concentration detectable by ¹H NMR. The conversion of 4VP to P4VP in the second polymerisation step could not be calculated as the unreacted monomer was removed during the CO₂ extraction step prior to analysis.

Molecular weight of the block copolymers was determined by a combination of GPC and ¹H NMR. Molecular weight of the PMMA macro-RAFT agents was determined by GPC analysis calibrated against PMMA narrow standards, with calculated *M_n* values close to the target value of 50 kg mol⁻¹ in all case (Table 1). Low *D* were also demonstrated (<1.25). Due to the presence of AgNP in the final block copolymers, samples could not be analysed using GPC as it was feared damage may be caused to the chromatography column. Attempts to separ-

ate the out the AgNP by centrifugation and syringe filtration prove unsuccessful. Instead, molecular weights were determined by comparing the characteristic ¹H NMR peak integrals for each polymer block to calculate the weight fraction of P4VP in the copolymer (*w_{P4VP}*). Molecular weight of the copolymers was calculated using these values and the predetermined molecular weight of the PMMA blocks. This assumes 100% blocking efficiency of the PMMA macro-RAFT agent and cannot be used to determine *D* values.

Values of *w_{P4VP}* (Table 1) were found to be lower than the target value of 25% for all the block copolymers. This indicated that full conversion of the 4VP was not achieved even after 24 hours, contradicting results from our previous studies on the polymerisation of PMMA-*b*-P4VP in scCO₂.²⁴ This was certainly a result of the added Ag(hfac)(COD) in these polymerisations. It was likely that silver ions were responsible for partially quenching the controlled radical reaction, however, *w_{P4VP}* was not found to decrease with increasing quantity of Ag(hfac)(COD). Nevertheless, the determined molecular weight of all block copolymers was sufficiently high to enable self-assembly of the polymers into a spherical-type nanoscale morphology.²⁵

The microstructure of the composites was evaluated by SEM analysis (Fig. 1) with the average microparticle diameter (*d_n*) measured (Table 1) and the size dispersity reported as a coefficient of variation (CV) percentage. All the composites were found to somewhat retain the microparticle structure of the PMMA macro-RAFT agent seeds that are typically produced in a scCO₂ dispersion polymerisation.³⁶ Though, the definition of these microparticles was found to become slightly less well-defined as the quantity of Ag(hfac)(COD) in the reaction was increased. The lack of definition appeared to be due to the formation of smaller nanoscale particles on the surface of the original microparticles. This would be undesired P4VP homopolymer that was produced, rather than the 4VP being fully incorporated into the PMMA seed particles. This may have been caused by an increased amount of quenching of the controlled radical reaction as the quantity of silver in the reaction increased. This in turn could have favoured the homopolymerisation of P4VP and nucleation of additional smaller particles.

The internal microparticle structure was examined by TEM analysis of unstained thin particle cross-sections (Fig. 2). All the PMMA-*b*-P4VP microparticles were found to contain the

Table 1 Summary of polymer characterisation data for the PMMA-*b*-P4VP-AgNP block copolymer composite samples, synthesised with various amounts of Ag(hfac)(COD)^a

| Ag(hfac)(COD) loading (mg) | PMMA | | | PMMA- <i>b</i> -P4VP | | | |
|----------------------------|------------------------------------|---|------------------------------|---|--|--|------------------------------------|
| | Conversion ^{<i>b</i>} (%) | <i>M</i> _{n exp} ^{<i>c</i>} (kg mol ^{−1}) | <i>D</i> ^{<i>c</i>} | <i>M</i> _{n exp} ^{<i>b</i>} (kg mol ^{−1}) | <i>w</i> _{P4VP} ^{<i>b</i>} | <i>d</i> _n ^{<i>d</i>} (μm) | AgNP size ^{<i>e</i>} (nm) |
| 62.5 | 99 | 53.3 | 1.23 | 65.8 | 16 | 2.34 | 8.2 |
| 125 | 99 | 54.0 | 1.22 | 67.6 | 20 | 2.13 | 14.8 |
| 250 | 99 | 55.5 | 1.21 | 65.1 | 15 | 2.06 | 20.2 |

^a Conditions: 7.5 g of PMMA macro-RAFT seed dispersed with 0.125 g PDMS-MA and Ag(hfac)(COD) at 65 °C and 241 bar for 1 h, then 2.5 g of 4VP added for 24 h. ^b Obtained from ¹H NMR integrations. ^c Obtained from GPC, eluting in a chloroform/ethanol/TEA mixture, measured with dRI detector calibrated against PMMA narrow standards. ^d Measured from SEM images. ^e Obtained from DLS analysis in dichloromethane.



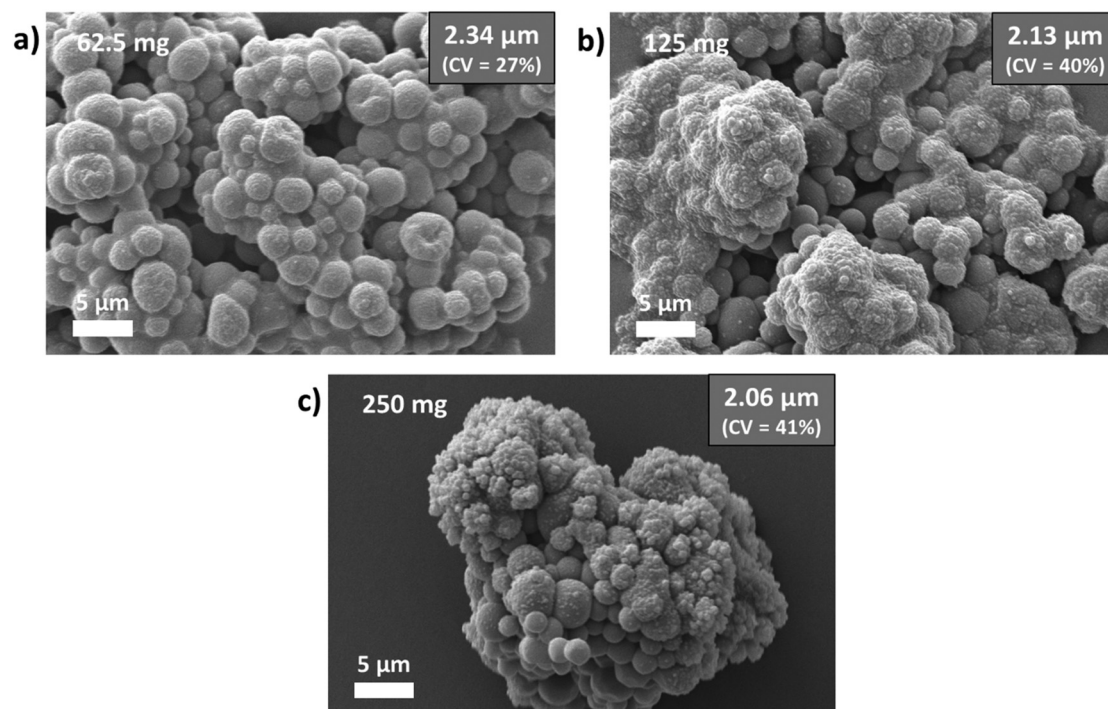


Fig. 1 SEM micrographs of the PMMA-*b*-P4VP-AgNP composites synthesised with (a) 62.5 mg, (b) 125 mg and (c) 250 mg of Ag(hfac)(COD) precursor.

expected spherical self-assembled block copolymer morphology, despite the omission of staining agents to enhance the contrast between the two polymer blocks. This indicates the successful chain extension of the macro-RAFT agent to a block copolymer, despite the lack of GPC data for the copolymers. TEM also revealed the presence of very small dark spots within the microparticles. This could only be the formed AgNP, as this was the only element present in the composites that was heavy enough to give such a dark contrast in the TEM images. The AgNP were found to be dispersed randomly and relatively evenly throughout the particle cross-sections. The only difference noted was in the case of the composite formed using the largest quantity of Ag(hfac)(COD). The AgNP in this composite were found to be significantly larger than the other composites and were undoubtedly a product of increased aggregation of the highly concentrated silver precursor.

To confirm that the presence of AgNP within the polymer particles was a direct result of the silver interaction with the 4VP monomer, a control experiment was performed. The control was synthesised by re-dispersing PMMA macro-RAFT seed particles in scCO_2 with 125 mg of Ag(hfac)(COD) at 65 °C. The addition of 4VP was omitted and after 24 hours the material was extracted with a flow of CO_2 for 30 minutes and collected as a brown, free-flowing powder. SEM and TEM analyses (Fig. S2†) confirmed the PMMA microparticle structure had been retained and that AgNP were formed only on the exterior or outer layer of the PMMA particles. The AgNP were too small to be noticeable in the SEM images and were only identified during the cross-sectional TEM analysis. This con-

firmed that composites with a homogeneous distribution of AgNP through the polymer could only be formed with the addition of 4VP moieties that directed the movement of Ag(hfac)(COD) into the PMMA seed particles.

The AgNP in the composites were further analysed by UV/vis spectroscopy and DLS (Fig. 3) to determine the relative concentration and average size of the nanoparticles (Table 2). Composite samples were dissolved in dichloromethane to fully dissolve the PMMA-*b*-P4VP, leaving only the AgNP dispersed in the solutions.

All UV/vis spectra revealed a sharp absorbance at around 310 nm, corresponding to the RAFT agent end group used in the synthesis of the block copolymer.³⁷ All spectra were then scaled to overlap the intensity of these peaks, as the concentration of this RAFT agent remained constant across all composite syntheses. A broad absorbance is seen at around 390–410 nm for all dissolved composites, relating to the surface plasmon absorbance of AgNP. This corresponds to AgNP of roughly <10 nm, as the energy of the surface plasmon is known to be size dependent.^{38,39} The absorbance intensity (Table 2) was shown to increase with increasing quantity of Ag(hfac)(COD), except in the case of the highest loading of 250 mg. It was predicted this was due to the larger AgNP observed in the TEM, and hence the effective number of AgNP for this composite was unlikely to have increased.

DLS confirmed the presence of small AgNP in the composites (8.2–20.2 nm), with size increasing slightly at higher loading of Ag(hfac)(COD). All measured nanoparticles show reasonably low polydispersity (PDI) (Table 2), with PDI quoted



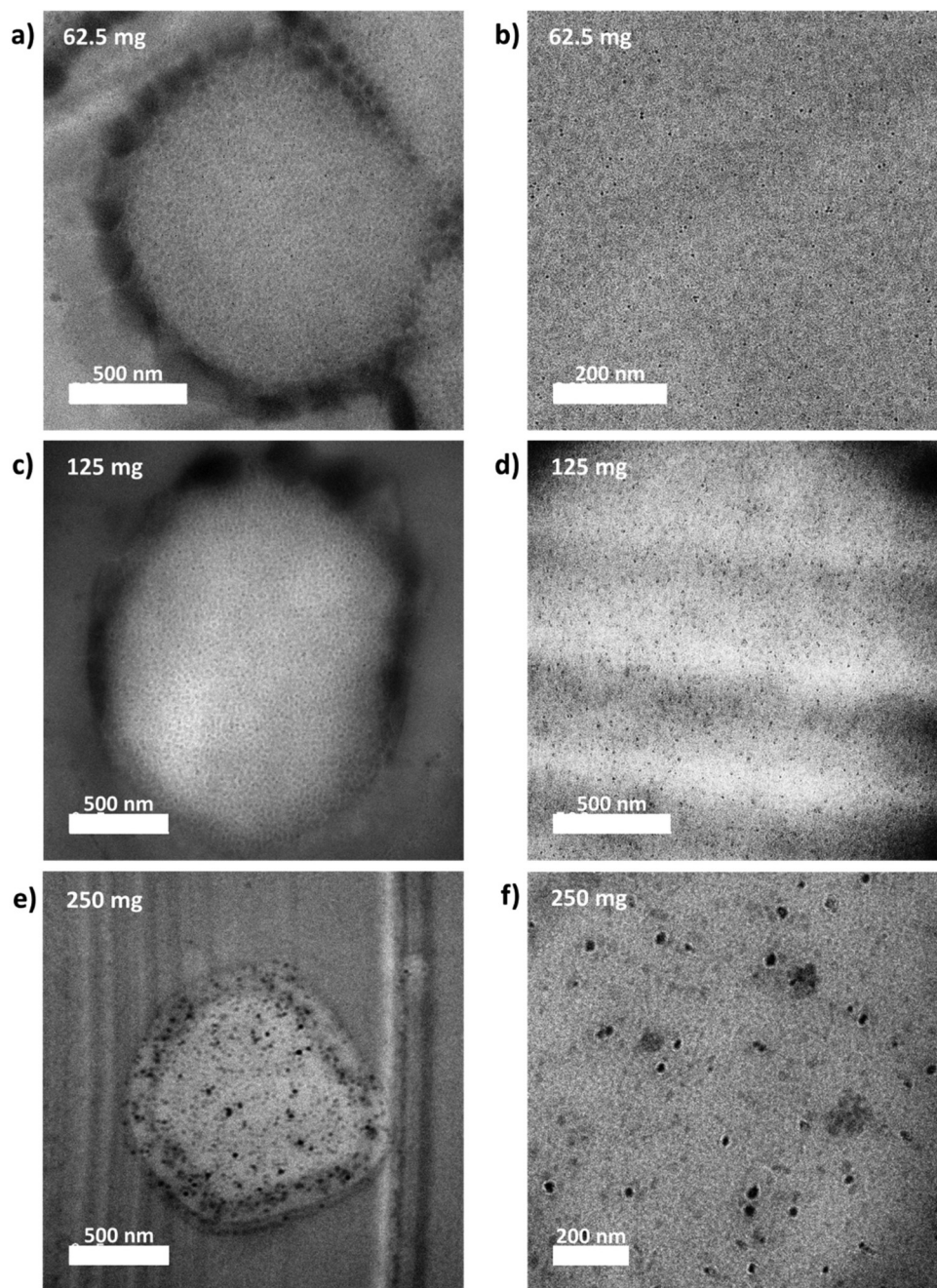


Fig. 2 TEM cross-sectional micrographs of the PMMA-*b*-P4VP-AgNP composites, synthesised using (a and b) 62.5 mg, (c and d) 125 mg and (e and f) 250 mg of Ag(hfac)(COD) precursor.

as the standard deviation squared divided by d_n^2 . This was done to avoid contribution of the aggregate peaks. These small AgNP accounted for >90% of the total particle volume measured, with the remaining volume appearing as very shallow peaks at >30 nm. We speculate that these larger particles may be aggregates of the smaller AgNP, as no particle stabilising agents were used when dissolving the composites in dichloromethane.

DSC and TGA were used to fully assess the thermal properties of the composites. DSC (Fig. S3a†) revealed only a

single step transition of the composites, matching most closely to the T_g of the PMMA. No T_g was observed for the P4VP. It was expected this was due to the relatively low quantity of the polymer block in the composite. The PMMA T_g in the composites was found to decrease from that observed in the neat PMMA-*b*-P4VP block copolymer (Table 2), with a larger decrease seen with increasing amount of Ag(hfac)(COD). Such a trend has been observed in polymers loaded with nanofillers, with more nanoparticles further enhancing polymer chain mobility and thus reducing the energy required to tran-



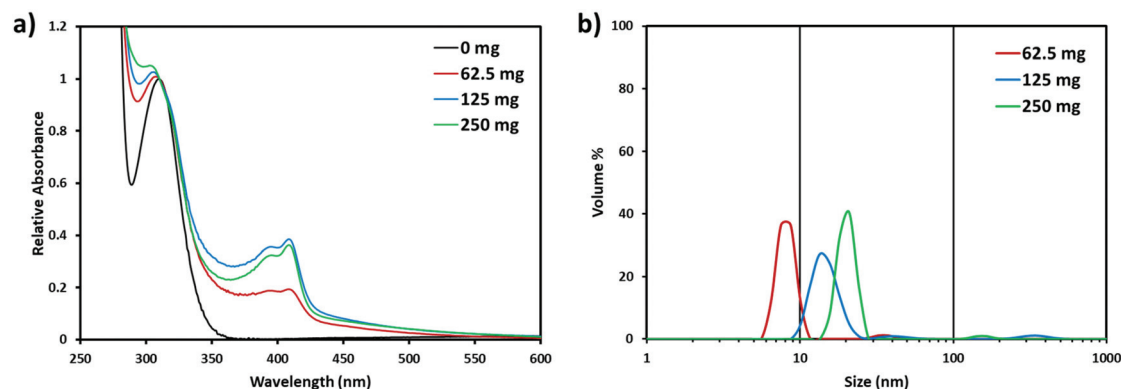


Fig. 3 (a) UV-vis spectra and (b) DLS plots of the composite samples dissolved in dichloromethane.

Table 2 Summary of the characterisation data for the PMMA-*b*-P4VP-AgNP block copolymer composite samples, synthesised with various quantities of Ag(hfac)(COD)

| Ag(hfac)(COD) loading (mg) | PMMA T_g^a (°C) | AgNP size ^b | | Relative absorbance at ^c 410 nm |
|-------------------------------|----------------------|--------------------------------|-------|--|
| | | Average size, d_n (nm) | PDI | |
| 0 | 125 | N/A | N/A | 0 |
| 62.5 | 117 | 8.2 | 0.016 | 0.19 |
| 125 | 107 | 14.8 | 0.038 | 0.38 |
| 250 | 89 | 20.2 | 0.015 | 0.36 |

^a Obtained DSC measurements. ^b Obtained from DLS measurements.

^c Obtained from UV-vis spectra.

sition to a rubber-like state.⁴⁰ A depression of the PMMA T_g would indicate that the AgNP are present in the PMMA block copolymer phase rather than exclusively in the P4VP domains. Though it should be noted that DSC data was obtained on the second heating cycle of the samples and the AgNP may have migrated to the PMMA domains during the first heat cycle.

TGA profiles (Fig. S3b†) of the sample degradation under an air atmosphere up to 700 °C were identical, regardless of the amount of Ag(hfac)(COD) used in the synthesis. The onset of thermal degradation of the polymers was found to be around 280 °C in all cases and confirmed that the added AgNP did not alter the thermal stability of the block copolymer. All samples were found to contain a small amount (~2 wt%) of black material after heating isothermally for 1 hour. This was expected to be mostly elemental silver, with a small amount of non-combusted polymer. Due to the very small quantity of residual material and the presence of other carbon-based residues, the mass of this non-combusted material could not be used to determine the quantity of AgNP in the composites.

Biocompatibility and antimicrobial activity

Though the initial ¹H NMR analysis demonstrated the success of the CO₂ extraction procedure in removing potentially toxic organic by-products, more rigorous tests were performed to

confirm the lack of cytotoxicity in the end materials. The cytocompatibility of the polymer composites was tested against a Caco-2 intestinal epithelial cell line, with the composite powder suspended directly in the culture media. Cell viability assessed using a PrestoBlue® assay to determine metabolic activity and by measurement of lactate dehydrogenase (LDH) release from the cells as an indicator for cell membrane integrity (Fig. 4). Tests were performed in triplicate along with a control experiment using Triton X-100 detergent to model cell death and a negative sample set containing only the cultured cells.

The data demonstrate lack of cytotoxicity of the block copolymer and composites synthesised using the lower amounts of Ag(hfac)(COD), as indicated by no decreases in cellular metabolic activity or cell membrane disruption as measured by extracellular release of LDH. However, the composite made using 250 mg of the silver precursor did induce a reduction in metabolic activity to approx. $71 \pm 6.2\%$ and substantial LDH release of $67 \pm 7.8\%$. Together these measurements indicate that this particular composite was cytotoxic and would not be biocompatible in its current form. This may be a result of trace amounts of precursor ligands remaining in the composite, likely resulting from significantly high concentration of these molecules in this reaction. To generate this material in non-cytotoxic manner, a longer and more thorough CO₂ extraction process would need to be applied.

The materials that proved to be non-cytotoxic (62.5 and 125 mg) were then tested for their antimicrobial activity against two Gram-positive bacterial species (*Staphylococcus aureus* and *Staphylococcus epidermidis*). Composite powders (and ordinary PMMA-*b*-P4VP) were suspended in sterilised water, then 10 µL aliquots of the supernatants were taken at various timepoints and placed on Muller Hinton agar plates seeded with the different bacterial strains. Agar plates were incubated for 18 hours before visually inspected the plates for signs of bacterial growth inhibition (Fig. S4†). Inhibition was measured by the diameter of the halo around the area the supernatant droplet was deposited (Table 3).

The supernatants of the composite dispersion taken after mixing for 24 hours showed no activity against any bacterial



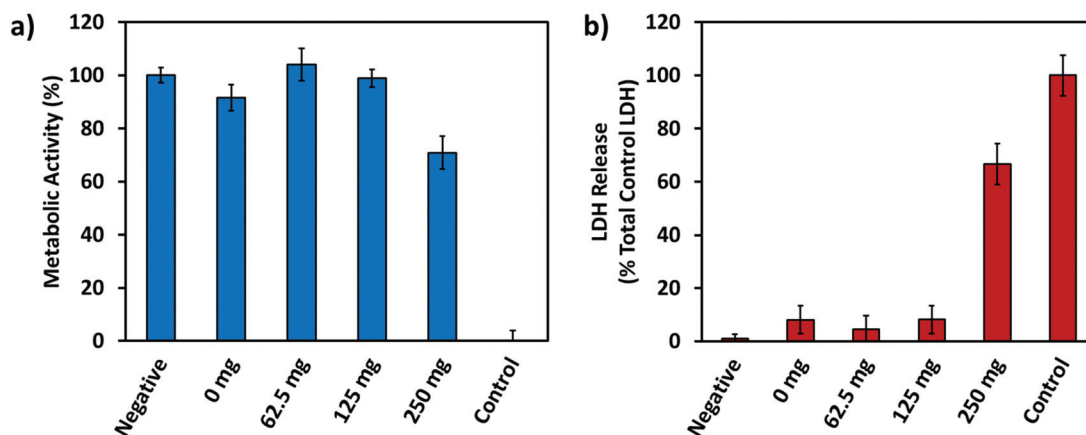


Fig. 4 Biocompatibility tests of PMMA-*b*-P4VP-AgNP samples with Caco-2 intestinal epithelial cells. Measurement of cell (a) metabolic activity and (b) LDH release after exposure to samples for 48 h. Negative group is untreated control and control group is Triton X-100 treated cells to induce cell death. Tests conducted in triplicate. Data presented as mean \pm S.D. Values on x-axis relate to quantity of Ag(hfac)(COD) used in the synthesis.

Table 3 Summary of antimicrobial test results

| Microorganism | Diameter of inhibition halo (mm) | | | | | |
|------------------------------------|----------------------------------|--------|--------------------------|-----------|---------------------------|------------|
| | Supernatant after 1 day | | Supernatant after 2 days | | Supernatant after 15 days | |
| | 62.5 mg | 125 mg | 62.5 mg | 125 mg | 62.5 mg | 125 mg |
| <i>S. aureus</i> (10850) | 0 | 0 | 9 \pm 1 | 9 \pm 1 | 9 \pm 1 | 9 \pm 1 |
| <i>S. epidermidis</i> (ATCC 35984) | 0 | 0 | 0 | 0 | 10 \pm 1 | 10 \pm 1 |

strain, irrespective of AgNP loading. However, after 48 hours waters from both composites showed clear signs of inhibiting the growth of the *S. aureus* 10850 strain. This same effect was observed after extracting the supernatant for the mixture after stirring for 15 days, with additional inhibition noted this time for the *S. epidermidis* ATCC 35984 strain. No inhibition was observed for the PMMA-*b*-P4VP powder against either bacterial strain, demonstrating that the antimicrobial activity of the composites was solely a result of the AgNP component.

It is likely that the AgNP are released very slowly from the block copolymer microparticles in the aqueous media, resulting in no immediate antimicrobial activity. However, after around 48 hours the concentration of released AgNP in the waters would appear to be high enough to inhibit the growth of Gram-positive bacteria. This slow and prolonged release of AgNP for the polymer particles ensures the antimicrobial activity of the waters is extremely long-lived, with activity persisting beyond two weeks. This highly sought-after ability to prolong antimicrobial activity could give these composites application in more long-term medical treatments.⁴¹

To confirm that this long-term antimicrobial activity was indeed the result of released AgNP, a release study for the 125 mg composite was performed by suspending the powder in water. UV/vis spectra collected from aliquots at various time-point (Fig. S5a†) show a gradual increase in intensity of the Ag surface plasmon peak at around 400 nm over a 3-day period. This supports the assertion that AgNP are released from the

composites into the water slowly and likely reach a critical concentration after several days where they begin to possess significant antimicrobial activity. The same release study was also performed in a pH 4.7 aqueous buffer solution (Fig. 5b). A similar trend of increasing Ag plasmon absorbance over time was observed, however, the intensity of this absorbance was slightly less than the study in neutral water. This serves to highlight how the AgNP release from the composites could be expected to change in a physiological environment, perhaps reducing the antimicrobial efficacy of the composites. Though, an exact model of release in a physiological environment cannot be properly modelled here *in vitro* due to the extremely high number of variables involved. An *in vivo* experiment would be required to accurately determine the efficacy of these composites in the human body.

Composite compatibility with laser sintering

Finally, the composite powders were tested for their suitability as a construction material in LS. The inherent microparticulate structure of the composite powders, from the dispersion polymerisation process, lends itself well to the LS technique. The AgNP composite synthesised using 125 mg precursor was spread over a LS build platform and sintered into a solid object by agglomerating the polymer particles using the heat provided by a CO₂ laser. Several small squares (20 \times 20 \times 0.5 mm) were constructed and collected for analysis (Fig. 5a insert). An approximate powder surface temperature of 150 $^{\circ}$ C



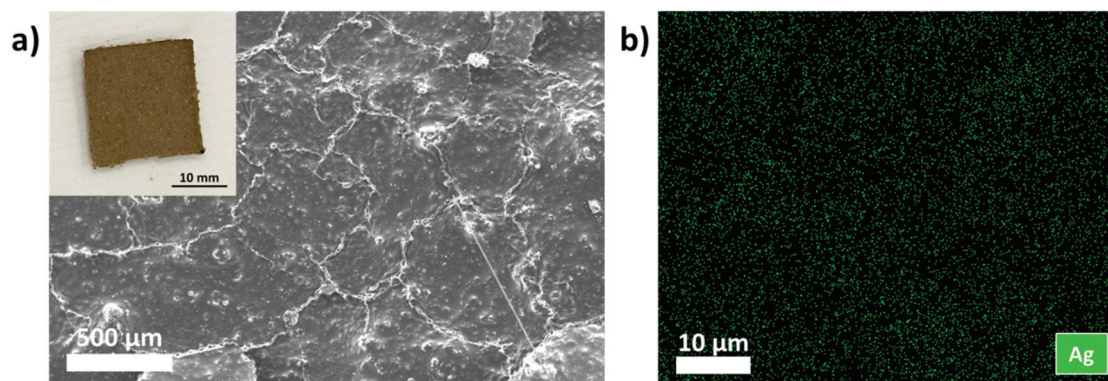


Fig. 5 (a) SEM micrograph of the SLS printed PMMA-*b*-P4VP-AgNP object (pictured in the insert, scale bar equal to 10 cm) and (b) EDXS elemental map of the same object, with elemental Ag signal displayed (green).

was recorded by the LS printer during the laser sintering process. This was significantly higher than the T_g measured for this composite (107 °C).

The objects were found to be quite brittle (in part due to being only a 0.5 mm thick single sintered layer) but did maintain their printed shape when manipulated and presented no visible signs of warping. The surface topography of the printed sample was investigated by SEM (Fig. 5a). Images revealed the surface to be relatively smooth, however, clear microfractures were also visible. Some small remnants of the original microparticle structure were also visible, but the overall surface was clearly a continuous solid. This initial test demonstrates that the synthesised composite can be utilised in LS to produce macro-scale products. Optimisation of the printing parameters or incorporation of additional polymeric filler will need to be investigated further to remove these imperfections and yield a more mechanically robust device.

The homogeneous distribution of the AgNP in the printed object was confirmed by EDXS mapping during SEM analysis (Fig. 5b), and by ToF-SIMS depth profiling (Fig. S6†). The full EDXS profile (Fig. S7†) showed the presence of locally high concentrations of silicon and oxygen around the unsintered microparticles, and this can be ascribed to the presence on the surface of the PDMS-MA stabiliser. Elemental silver was detected throughout the scanned area and appeared to be distributed homogeneously across the sample surface. ToF-SIMS revealed the presence of mass fragments relating to the PDMS-MA stabiliser (SiC_3H_9^+ , $\text{Si}_2\text{C}_5\text{H}_{15}\text{O}^+$) in high concentration at the surface of the printed object, as well as the unprinted microparticles. The concentration of these fragments quickly reduced with sample depth (sputter time), being replaced by fragments relating to PMMA, P4VP and Ag^+ . After a sputter time of around 150 s, the intensity of Ag^+ fragments became stable, indicating a constant Ag content across the bulk sample depth. Overall, the complementary techniques proved the homogeneous distribution of silver in the final printed product, reflecting the morphology of the original powder.

The silver component of the printed object was studied further by dissolving the object completely in dichloro-

methane. This was then examined *via* UV/vis spectroscopy and DLS (Fig. S8†) to reveal the presence of AgNP in the resulting solution. AgNP were found to be roughly the same size (11.8 nm) as in the pre-sintered powdered composite (14.8 nm). This confirms that the elemental silver detected in the other analyses remains primarily in its nanoparticulate antimicrobial form, even after the heat treatment and printing with the SLS laser. The retention of the AgNP during printing was likely influenced by the homogeneous nature of the composite particles. It would be expected that AgNP concentrated on the particle surface would be much more susceptible to agglomeration during the thermal sintering process.⁴² Therefore, these composite microparticles may be the only reported material compatible with the LS process to produce a AgNP-based product.

Finally, the release of AgNP from the printed sample was measured by submerging the sample in water and measuring the UV/vis spectra of aliquots taken at various timepoints (Fig. S9†). No AgNP were detected for the first 2 days of the release study. However, after 6 days a clear Ag surface plasmon absorption peak could be seen. The slower release of AgNP from the initial printed composite is likely due to the dramatically reduced surface area of the composite with the release media. As such, in its current form, this proof-of-concept printed object will not possess the same antimicrobial activity as the original composite powder. However, the successful release of some AgNP after printing means that in the future antimicrobial activity could be modified, for example, by incorporating added porosity or surface texture into the build, to alter the release rate.

Overall, the analysis shows the printed sample to be virtually identical to the powdered composite, with AgNP dispersed throughout. The release of AgNP from the printed sample still occurs after sintering, though at a reduced rate, likely due to the reduction in surface area from the original powder. Further printing studies are needed to confirm the exact effect of print geometry on the timeframe of antimicrobial activity, and to fully optimise the mechanical properties of the printed objects. We would also expect that there



would be additional benefits such as anti-attachment properties that would enhance the utility of our new materials and these should also be investigated in our future studies.

Conclusion

In summary, we have demonstrated a new low environmental impact synthetic methodology for producing homogeneous PMMA-*b*-P4VP-AgNP composite microparticles, that can reasonably be achieved in a one-pot scCO₂ process. A control experiment using only PMMA proved that a homogeneous distribution of AgNP within the polymer could only be achieved by addition of the P4VP component. Upon applying a 30-minute CO₂ extraction process post-synthesis, composites were found to have high purity and most had good cytocompatibility with Caco-2 intestinal epithelial cells. These composites were found to have a strong antimicrobial effect against two bacterial strains. Though this effect was initially delayed, the antimicrobial activity then proved to be extremely long-lived, surpassing the 15-day time period of the experiment.

Finally, the microparticulate nature of the composites was exploited for trial use in the SLS additive manufacturing process to successfully yield several small objects. The microparticles were shown to be well-sintered with a homogeneous distribution of AgNP throughout both the surface and depth of the object, much like the original particles. The size of the AgNP was also found to be reasonably unaffected by the sintering process. Further optimisation of the printing process is now needed to produce structures with the necessary mechanical properties for end use, while maintaining the high concentration of released AgNP. Full biological evaluation of these optimally printed materials will also be performed, including the anti-attachment properties of these new surfaces. If this proves to be as successful as the results for the neat microparticulate powders present here, it is expected that these new composites will prove to be incredibly valuable for use in the fabrication of novel bespoke medical devices.

Conflicts of interest

There are no conflicts to declare.

Acknowledgements

We would like to thank the Engineering and Physical Science Research Council (EPSRC) for their support of this project, as part of the Low Dimensional Materials and Interfaces (LDMI) doctoral training programme (EP/N50970X/1). The authors would also like to thank the Nanoscale and Microscale Research Centre (nmRC) at the University of Nottingham for access to electron microscope instruments and sample preparation equipment. Finally, we would like to thank Mr Richard Wilson and Mr Mark Guyler for their technical support with the high-pressure equipment.

References

- 1 X.-F. Zhang, Z.-G. Liu, W. Shen and S. Gurunathan, *Int. J. Mol. Sci.*, 2016, **17**, 1534.
- 2 A. Syafiuddin, Salmiati, M. R. Salim, A. Beng Hong Kueh, T. Hadibarata and H. Nur, *J. Chin. Chem. Soc.*, 2017, **64**, 732–756.
- 3 M. Sabela, S. Balme, M. Bechelany, J.-M. Janot and K. Bisetty, *Adv. Eng. Mater.*, 2017, **19**, 1700270.
- 4 Z.-J. Jiang, C.-Y. Liu and L.-W. Sun, *J. Phys. Chem. B*, 2005, **109**, 1730–1735.
- 5 A. Bouafia, S. E. Laouini, A. S. A. Ahmed, A. v. Soldatov, H. Algarni, K. Feng Chong and G. A. M. Ali, *Nanomaterials*, 2021, **11**.
- 6 O. Gherasim, R. A. Puiu, A. C. Bîrcă, A.-C. Burduşel and A. M. Grumezescu, *Nanomaterials*, 2020, **10**, 2318.
- 7 I. X. Yin, J. Zhang, I. S. Zhao, M. L. Mei, Q. Li and C. H. Chu, *Int. J. Nanomed.*, 2020, **15**, 2555–2562.
- 8 S. S. Jeremiah, K. Miyakawa, T. Morita, Y. Yamaoka and A. Ryo, *Biochem. Biophys. Res. Commun.*, 2020, **533**, 195–200.
- 9 N. S. Tulve, A. B. Stefaniak, M. E. Vance, K. Rogers, S. Mwilu, R. F. LeBouf, D. Schwegler-Berry, R. Willis, T. A. Thomas and L. C. Marr, *Int. J. Hyg. Environ. Health*, 2015, **218**, 345–357.
- 10 A. A. Yaqoob, K. Umar and M. N. M. Ibrahim, *Appl. Nanosci.*, 2020, **10**, 1369–1378.
- 11 S. Iravani, H. Korbekandi, S. v. Mirmohammadi and B. Zolfaghari, *Res. Pharm. Sci.*, 2014, **9**, 385–406.
- 12 A. Roy, O. Bulut, S. Some, A. K. Mandal and M. D. Yilmaz, *RSC Adv.*, 2019, **9**, 2673–2702.
- 13 C. Vanlalveni, S. Lallianrawna, A. Biswas, M. Selvaraj, B. Changmai and S. L. Rokhum, *RSC Adv.*, 2021, **11**, 2804–2837.
- 14 R. Vishwanath and B. Negi, *Curr. Res. Green Sustainable Chem.*, 2021, **4**, 100205.
- 15 X. Ye and C. M. Wai, *J. Chem. Educ.*, 2003, **80**, 198.
- 16 Y. Zhang and C. Erkey, *J. Supercrit. Fluids*, 2006, **38**, 252–267.
- 17 E. Izak-Nau, A. Huk, B. Reidy, H. Uggerud, M. Vadset, S. Eiden, M. Voetz, M. Himly, A. Duschl, M. Dusinska and I. Lynch, *RSC Adv.*, 2015, **5**, 84172–84185.
- 18 J. M. Gorham, A. B. Rohlfing, K. A. Lippa, R. I. MacCuspie, A. Hemmati and R. David Holbrook, *J. Nanopart. Res.*, 2014, **16**, 2339.
- 19 K. S. Morley, P. C. Marr, P. B. Webb, A. R. Berry, F. J. Allison, G. Moldovan, P. D. Brown and S. M. Howdle, *J. Mater. Chem.*, 2002, **12**, 1898–1905.
- 20 J. Yang, T. Hasell, D. C. Smith and S. M. Howdle, *J. Mater. Chem.*, 2009, **19**, 8560–8570.
- 21 T. Hasell, L. Lagonigro, A. C. Peacock, S. Yoda, P. D. Brown, P. J. A. Sazio and S. M. Howdle, *Adv. Funct. Mater.*, 2008, **18**, 1265–1271.
- 22 R. Kumar, S. Howdle and H. Münstedt, *J. Biomed. Mater. Res., Part B*, 2005, **75**, 311–319.
- 23 T. Hasell, K. J. Thurecht, R. D. W. Jones, P. D. Brown and S. M. Howdle, *Chem. Commun.*, 2007, 3933–3935.



- 24 J. Jennings, M. Beija, A. P. Richez, S. D. Cooper, P. E. Mignot, K. J. Thurecht, K. S. Jack and S. M. Howdle, *J. Am. Chem. Soc.*, 2012, **134**, 4772–4781.
- 25 J. Jennings, S. P. Bassett, D. Hermida-Merino, G. Portale, W. Bras, L. Knight, J. J. Titman, T. Higuchi, H. Jinnai and S. M. Howdle, *Polym. Chem.*, 2016, **7**, 905–916.
- 26 G. He, T. M. Bennett, K. Alias, L. Jiang, S. T. Schwab, M. Alauhdin and S. M. Howdle, *Polym. Chem.*, 2019, **10**, 3960–3972.
- 27 T. M. Bennett, G. He, R. R. Larder, M. G. Fischer, G. A. Rance, M. W. Fay, A. K. Pearce, C. D. J. Parmenter, U. Steiner and S. M. Howdle, *Nano Lett.*, 2018, **18**, 7560–7569.
- 28 R. R. Larder, T. M. Bennett, L. S. Blankenship, J. A. Fernandes, B. K. Husband, R. L. Atkinson, M. J. Derry, D. T. W. Toolan, H. A. Centurion, P. D. Topham, R. v. Gonçalves, V. Taresco and S. M. Howdle, *Polym. Chem.*, 2021, **12**, 2904–2913.
- 29 A. Awad, F. Fina, A. Goyanes, S. Gaisford and A. W. Basit, *Int. J. Pharm.*, 2020, **586**, 119594.
- 30 R. D. Turner, J. R. Wingham, T. E. Paterson, J. Shepherd and C. Majewski, *Sci. Rep.*, 2020, **10**, 892.
- 31 M. Alauhdin, T. M. Bennett, G. He, S. P. Bassett, G. Portale, W. Bras, D. Hermida-Merino and S. M. Howdle, *Polym. Chem.*, 2019, **10**, 860–871.
- 32 ISO – International Organization of Standardization, *ISO 10993-5 – Biological Evaluation of Medical Devices. Part 5: Tests for in vitro cytotoxicity*, ISO, 3rd edn, 2009.
- 33 T. Hasell, L. Lagonigro, A. C. Peacock, S. Yoda, P. D. Brown, P. J. A. Sazio and S. M. Howdle, *Adv. Funct. Mater.*, 2008, **18**, 1265–1271.
- 34 S. W. Ehrlich, G. C. Banikiotes and M. Mackles, *US Pat*, 3547809A, 1970.
- 35 P. Mulvaney, *Langmuir*, 1996, **12**, 788–800.
- 36 A. M. Gregory, K. J. Thurecht and S. M. Howdle, *Macromolecules*, 2008, **41**, 1215–1222.
- 37 J. Jennings, M. Beija, J. T. Kennon, H. Willcock, R. K. O'Reilly, S. Rimmer and S. M. Howdle, *Macromolecules*, 2013, **46**, 6843–6851.
- 38 S. Raza, W. Yan, N. Stenger, M. Wubs and N. A. Mortensen, *Opt. Express*, 2013, **21**, 27344–27355.
- 39 R. Desai, V. Mankad, S. Gupta and P. Jha, *Nanosci. Nanotechnol. Lett.*, 2012, **4**, 30–34.
- 40 A. Bansal, H. Yang, C. Li, K. Cho, B. C. Benicewicz, S. K. Kumar and L. S. Schadler, *Nat. Mater.*, 2005, **4**, 693–698.
- 41 P. Gao, X. Nie, M. Zou, Y. Shi and G. Cheng, *J. Antibiot.*, 2011, **64**, 625–634.
- 42 H. C. Kim, H. T. Hahn and Y. S. Yang, *J. Compos. Mater.*, 2012, **47**, 501–509.

